Electronic Supplementary Information for

Porosity-driven electrochemical divergence in structurally polymorphic 2D metal-organic frameworks for lithium-ion storage

*Ajay Ugale, Abhijeet Patil, Sauvik Saha, Augastus Camellus R B, Mukul Sharma, Vikash Yadav, and Nirmalya Ballav**

Department of Chemistry, Indian Institute of Science Education and Research (IISER), Pune - 411008, India

E-mail: nballav@iiserpune.ac.in

Experimental

Chemicals. Ethylenediamine (en) (≥99.5%) was purchased from Sigma-Aldrich, India. Sodium dodecyl sulphate (SDS) was obtained from Avra, India. Copper(II) acetate was purchased from BLDpharm, India. Cupric nitrate trihydrate ($Cu(NO_3)_2 \cdot 3H_2O$, ≥99.5%) was purchased from SDFCL. Tetrahydroxy-1,4-benzoquinone hydrate (>96%) was purchased from TCI, India. All chemicals were used directly without further purification. The deionized water (18.2 MΩ cm^{-1}) used in the experiments was generated by a Milli-Q water system.

Synthesis of p-Cu-THQ. Cupric nitrate trihydrate ($Cu(NO_3)_2 \cdot 3H_2O$) (~221 mg, 0.916 mmol) with 92µl ethylenediamine in 40 mL degassed water and Tetrahydroxy-1,4-benzoquinone hydrate (THQ) (120 mg, 0.696 mmol) in 40mL degassed water were dissolved separately and mixed under N_2 protection and vigorous stirring. The mixture was then kept for stirring on 500 RPM at a room temperature for 12 hours. The precipitate obtained was filtered and subsequently centrifuged with H_2O (200 mL) and acetone (100 mL) at 7800 rpm and then dried overnight in a vacuum oven at 80 °C for further testing and characterization.

Synthesis of d-Cu-THQ. Copper acetate $Cu(OAc)_2$ (~480 mg, 2.61 mmol) and sodium dodecyl sulphate (SDS, ~150 mg, 0.51 mmol) were dissolved in 300 mL of deionized water in a 500 mL conical flask. Tetrahydroxy-1,4-benzoquinone hydrate THQ (~300 mg, 1.74 mmol) was then added into above solution, and the suspension was sonicated at 50 °C for 30 min to achieve uniform dispersion. The mixture was subsequently maintained at 80 °C without agitation for 10 h to allow framework formation. The precipitate obtained was filtered and subsequently centrifuged with H_2O (200 mL), Ethanol (100 mL) and acetone (100 mL) at 7800 rpm and then dried overnight in a vacuum oven at 100 °C for further testing and characterization.

Characterizations. PXRD data were recorded at room temperature using a Malvern PANalytical Empyrean (3rd Gen) XRD instrument operating with Cu Kα radiation (λ = 1.54 Å); The surface morphologies were investigated by FEI Nova NanoSEM 450 FESEM and EDXS-elemental mapping was carried out with Bruker XFlash 6I30 by drop-casting the ethanolic dispersion of samples onto Si wafer; TEM images were recorded on drop casted samples (ethanolic dispersion) over a 200 mesh Cu grid using JEOL USA JEM-2200 FS Transmission Electron Microscope. Gas adsorption and desorption isotherms were collected at 77 K for N_2 gas and 195 K for CO_2 gas on the Micromeritics 3-FLEX and BelSorp-MAX-X

instruments respectively. Attenuated Total Reflectance-based Fourier Transform Infrared (ATR-FTIR) spectra for the as-prepared powder samples were collected in the range of 500 to 4000 cm^{-1} with a resolution of 4 cm^{-1} using a BRUKER ALPHA-T instrument. ATR-FTIR for the electrodes at different discharge/charge states were acquired on a Bruker INVENIO R spectrometer using a Platinum ATR (A225/Q) diamond accessory at 4 cm^{-1} resolution in the range of 1000 to 2000 cm^{-1}. Raman spectra (λ_{exc} = 632.8 cm^{-1}) were recorded at Raman microscope (LabRAM HR, HoribaJobinYvon) using a 50x objective lens (spectral resolution of the system is ~1 cm^{-1}); XPS spectra were recorded by using a ThermoFisher Scientific K ALPHA+. XPS of the electrodes at charged and discharged states were recorded by using monochromatized Al K_α X-ray source (E_{ex} = 1486.0 eV) with an EA15 hemispherical Energy analyser, manufactured by PREVAC (Poland).

Electrochemical Measurements. CR2032-type coin cells were used for all electrochemical measurements at room temperature. The synthesized p-Cu-THQ and d-Cu-THQ powders was mixed with a ketjen black and a Polyvinylidene fluoride (PVDF) binder with weight ratio (70:20:10) respectively in an N-methyl-2-pyrrolidone (NMP) solvent to form a homogeneous slurry. This slurry was coated onto a copper foil using a doctor blade technique, followed by drying at 60 °C overnight under vacuum. The mass loading of the p-Cu-THQ and d-Cu-THQ active materials in the electrodes was controlled to be around 0.8-0.9 mg cm^{-2}. Electrodes were cut into 16 mm diameter and assembled into CR2032-type coin cells with lithium metal as the counter electrode. 120 µl of 1M $LiPF_6$ in a 1:1:1 (Volume ratio) mixture of ethylene carbonate, dimethyl carbonate, and ethyl methyl carbonate (EC: DMC: EMC) was used as electrolyte.[1, 2] Glass fibre was used as separator. The coin cells were assembled in an argon-filled glove box (MBRAUN Unilab plus), maintaining H_2O and O_2 concentrations strictly below 0.1 ppm. Charge/discharge tests were recorded on Neware 4000 battery testing system at room temperature. Cyclic voltammetry (CV), Electrochemical impedance spectroscopy (EIS) and Galvanostatic intermittent titration technique (GITT) measurements were performed on BioLogic (SP-150e) potentiostat.

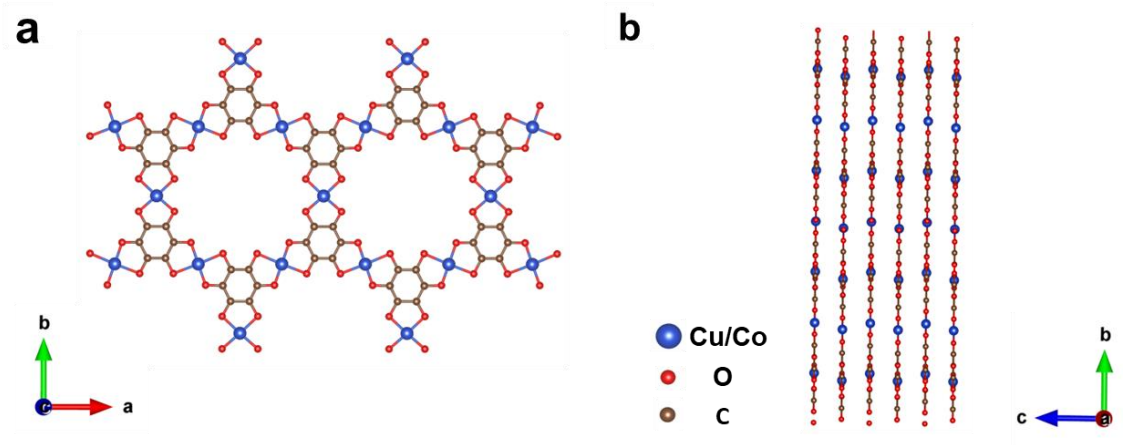

Figure S1. (a) 2D sheet of p-Cu-THQ in the ab-plane viewed from the crystallographic c-axis; **(b)** Slipped parallel AB stacking configuration of p-Cu-THQ layers viewed from a-axis.

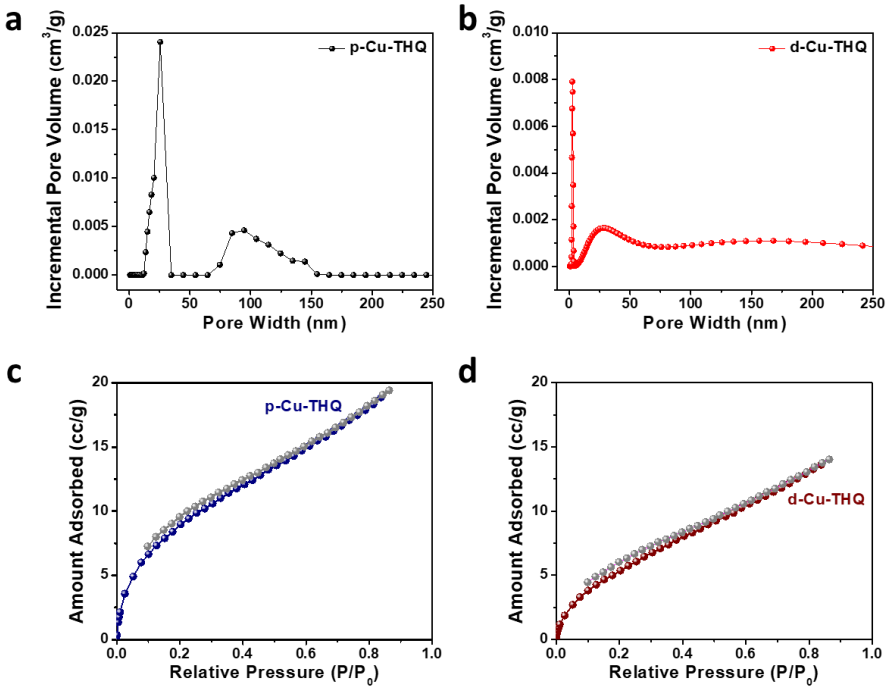

Figure S2. Pore-size distribution from N_2 sorption **(a)** p-Cu-THQ; **(b)** d-Cu-THQ and CO_2 adsorption-desorption isotherms of **(c)** p-Cu-THQ; **(d)** d-Cu-THQ at 195K.

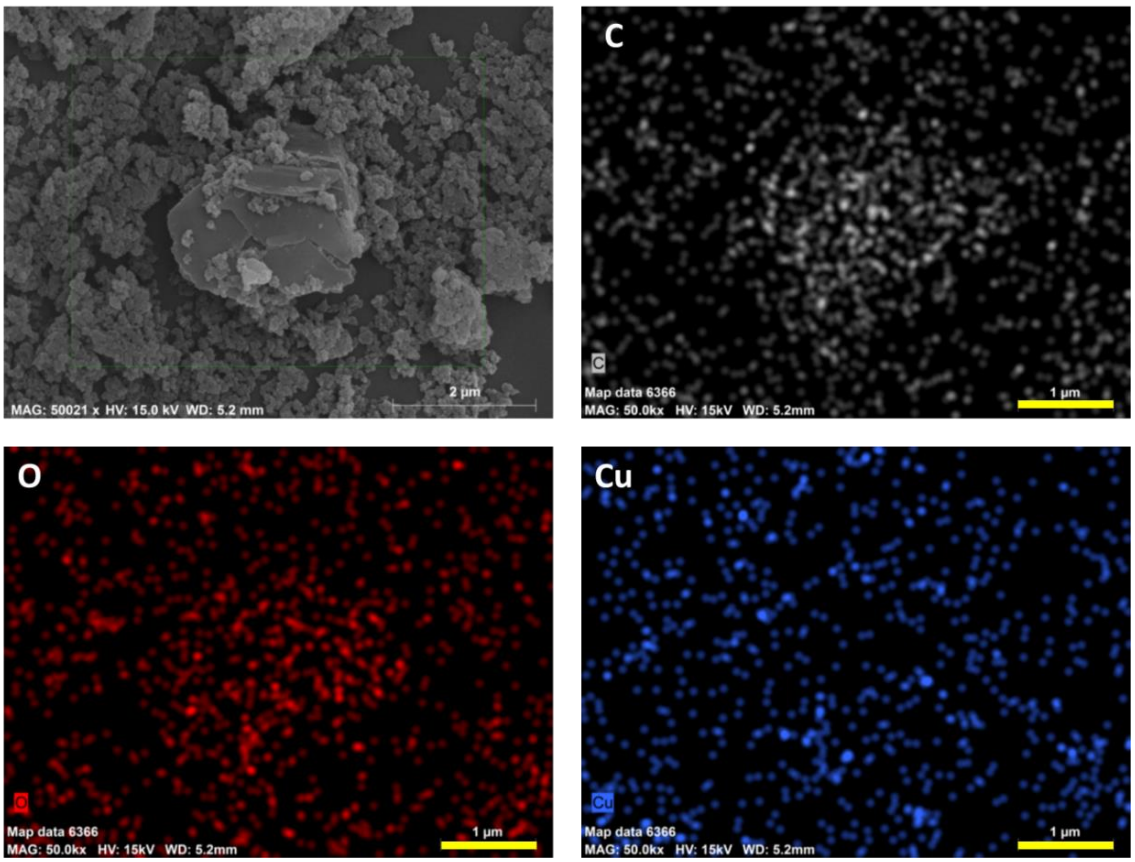

Figure S3. SEM image and elemental mapping of p-Cu-THQ.

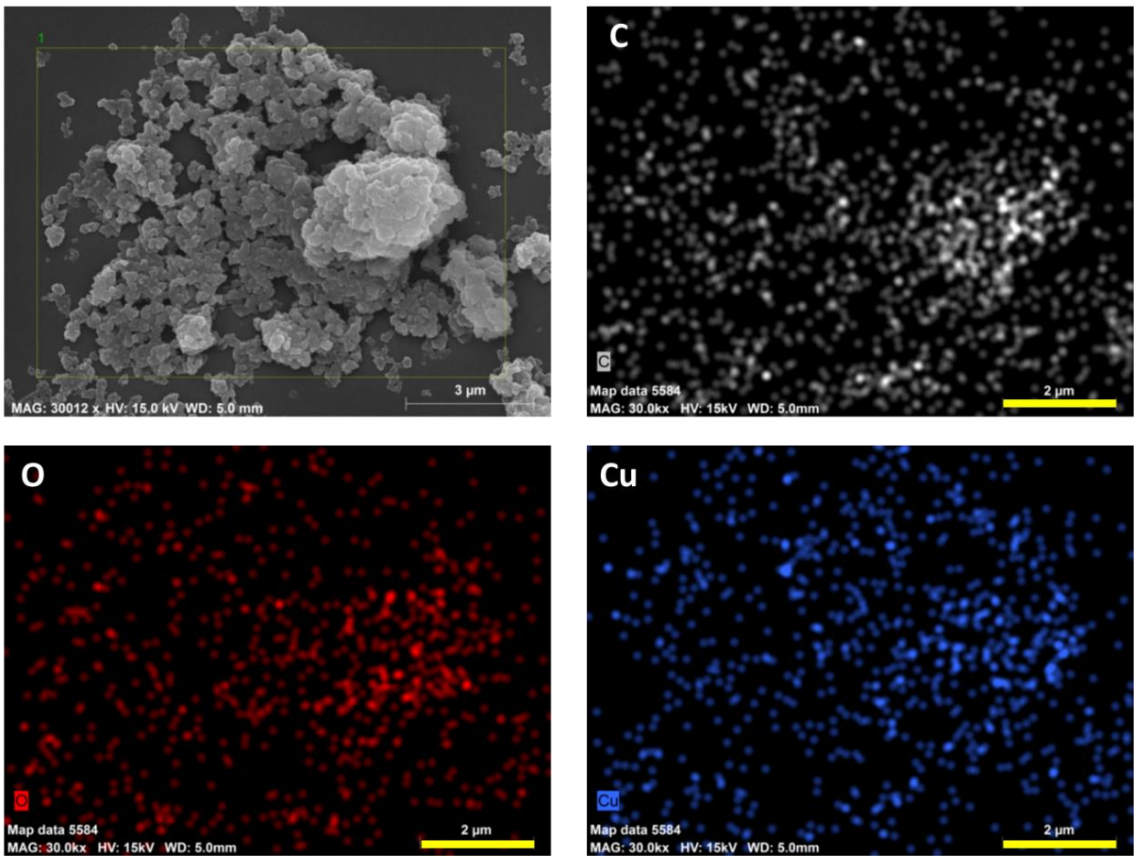

Figure S4. SEM image and elemental mapping of d-Cu-THQ.

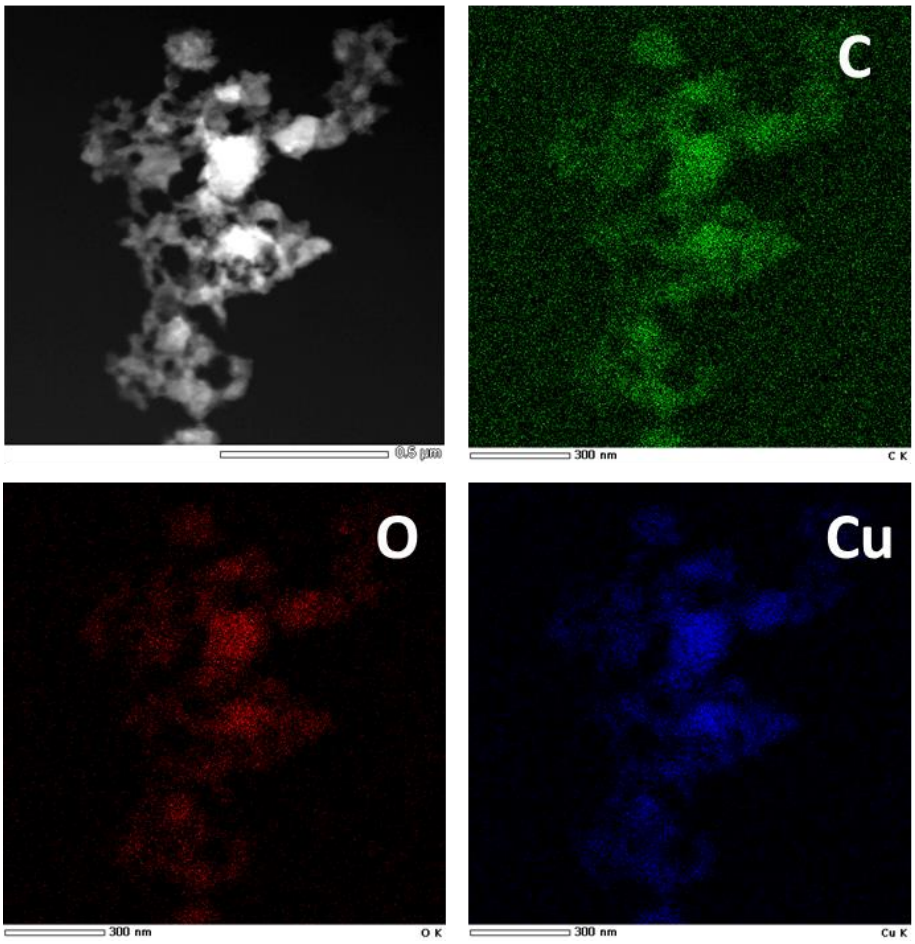

Figure S5. TEM image and elemental mapping of p-Cu-THQ.

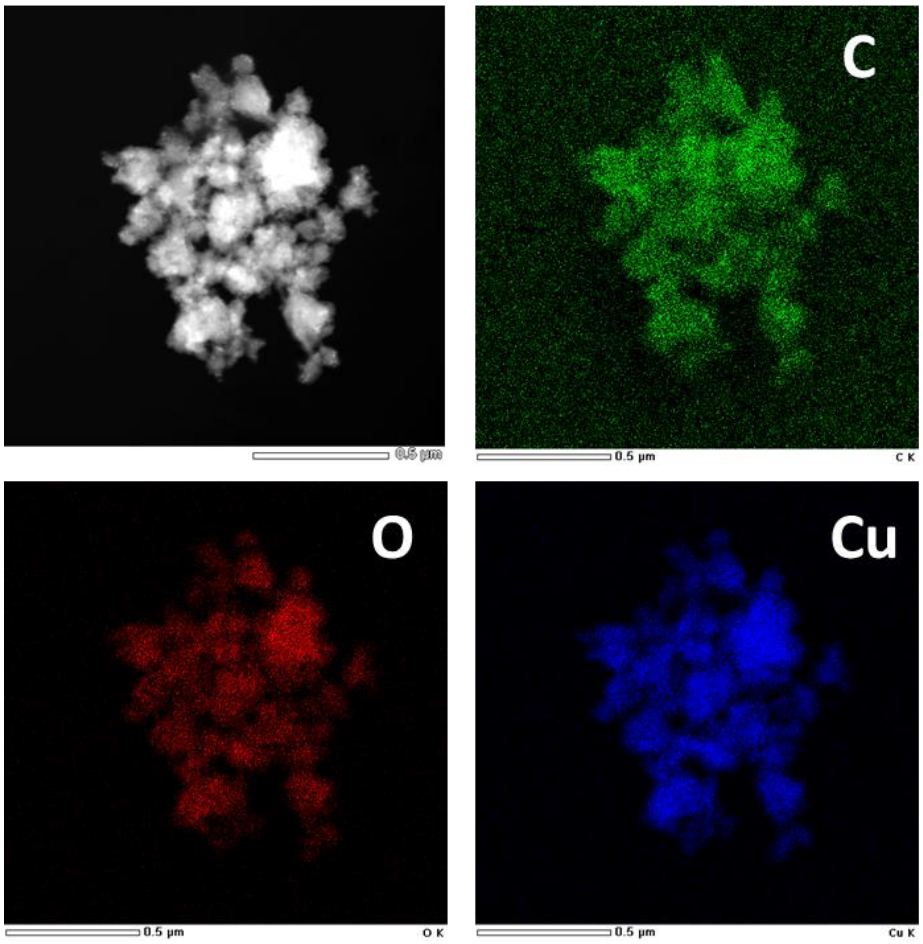

Figure S6. TEM image and elemental mapping of d-Cu-THQ.

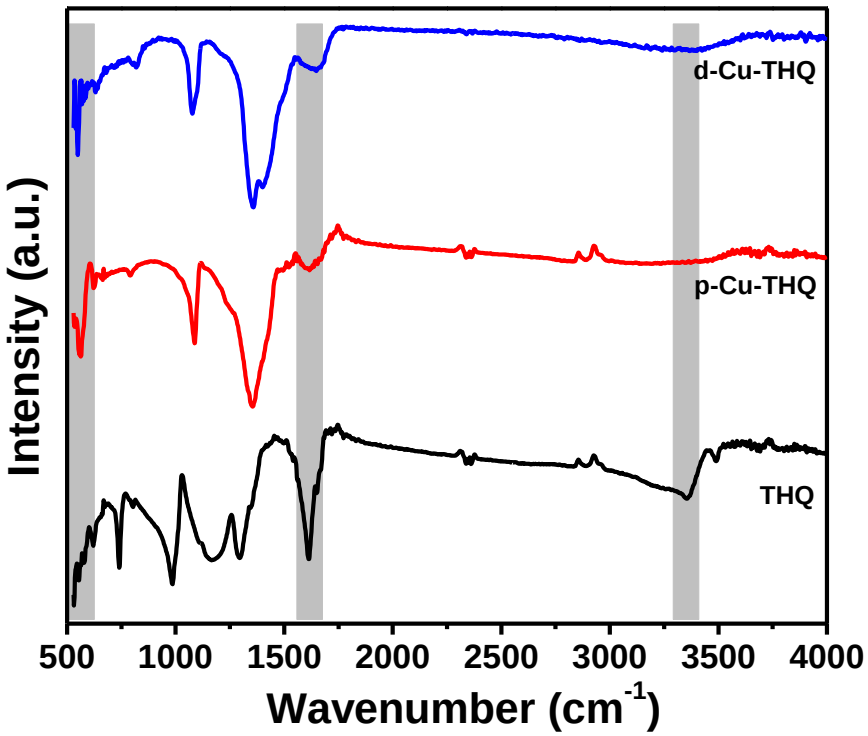

Figure S7. FTIR spectra of THQ, p-Cu-THQ and d-Cu-THQ.

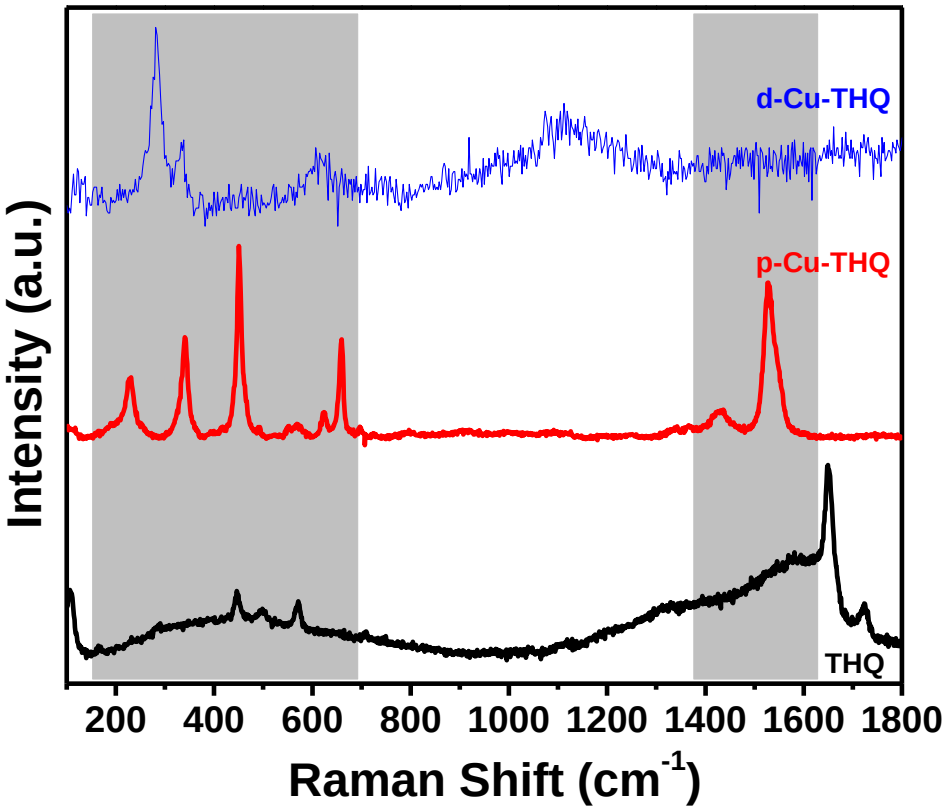

Figure S8. Raman spectra of THQ and p-Cu-THQ and d-Cu-THQ.

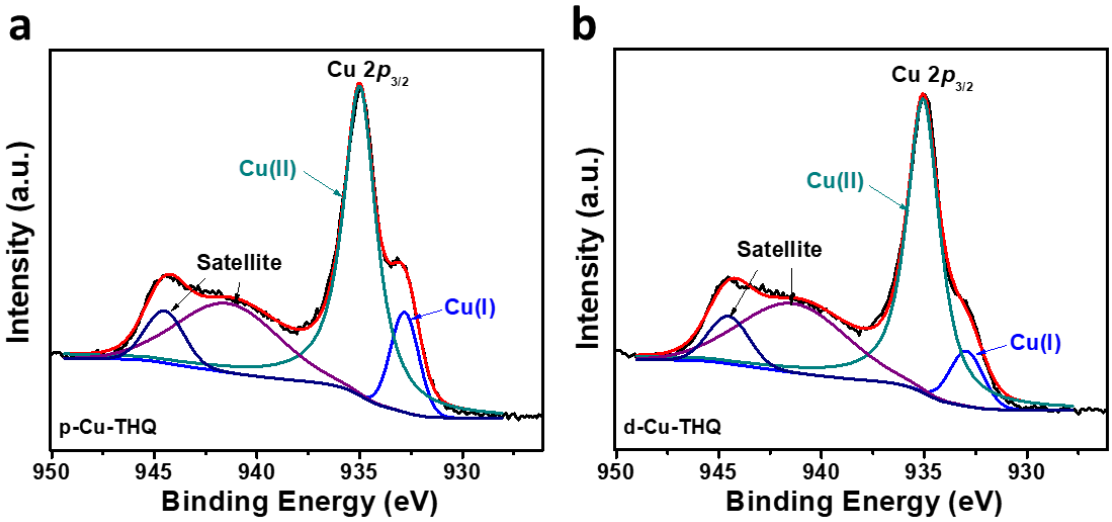

Figure S9. X-ray photoelectron spectroscopy signals of Cu2*p* for **(a)** p-Cu-THQ **(b)** d-Cu-THQ.

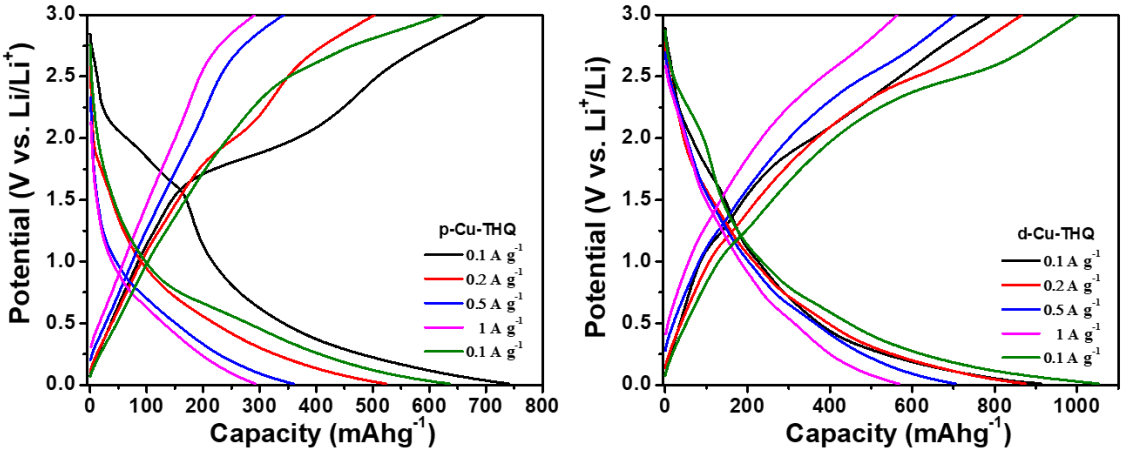

Figure S10. Charge-discharge curves of p-Cu-THQ and d-Cu-THQ under different current densities.

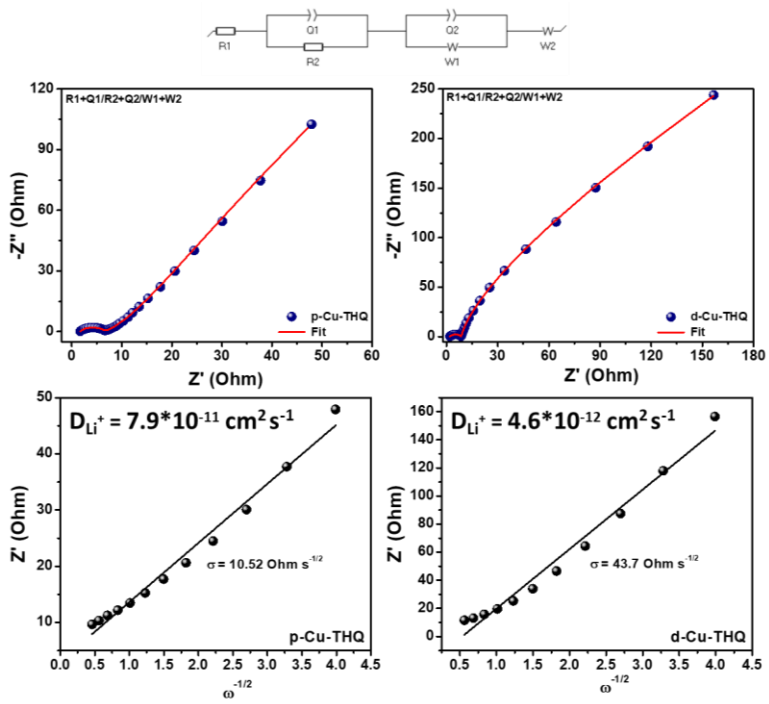

Figure S11. EIS spectra of fresh cells of p-Cu-THQ (left panel) and d-Cu-THQ (right panel) along with their D_{Li^+} values.

Electrochemical impedance spectroscopy (EIS) was carried out to investigate the lithium-ion transport kinetics and to determine the lithium diffusion coefficient (D_{Li^+}). The measurements were performed on freshly assembled cells in the frequency range from 1MHz to 10 mHz frequencies using a small AC perturbation amplitude (10mV). The obtained Nyquist plots consist of a depressed semicircle in the high-to medium-frequency region, attributed to the charge-transfer resistance (R_{ct}) and interfacial phenomena, followed by a straight line with a slope of ~45° in the low-frequency region, which corresponds to the Warburg impedance associated with solid-state diffusion of Li^+ ions within the electrode.

The lithium-ion diffusion coefficient (D_{Li^+}) was calculated from the Warburg coefficient using the following equation:

$$D = \frac{R^2T^2}{2A^2n^4F^4c^2\sigma^2}$$

Where R is the gas constant (8.314 J mol^{-1} K^{-1}), T is the absolute temperature, A is the effective electrode-electrolyte contact area, n is the number of electrons transferred per reaction, F is the Faraday constant (96485 C mol^{-1}), c is the molar concentration of lithium ions, and σ is the Warburg coefficient. The calculated D_{Li^+} values reflect the intrinsic lithium-ion diffusion kinetics within the electrode materials and enable a quantitative comparison of ion transport behaviour between different p-Cu-THQ and d-Cu-THQ electrode.

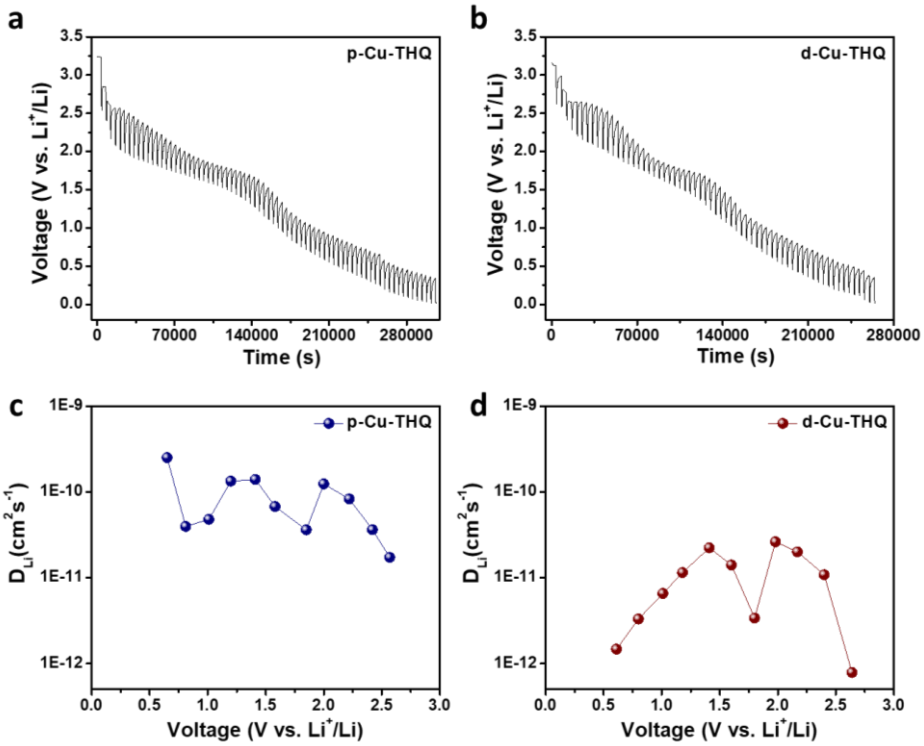

Figure S12. Galvanostatic intermittent titration technique (GITT) curves during discharge **(a)** p-Cu-THQ; **(b)** d-Cu-THQ and the corresponding lithium-ion diffusion coefficients (D_{Li^+}) values extracted at different voltages **(c)** p-Cu-THQ; **(d)** d-Cu-THQ.

Galvanostatic intermittent titration technique (GITT) measurements were carried out to evaluate the lithium-ion diffusion kinetics of the electrodes. The measurements were performed by applying a constant current pulse for 10 min, followed by an open-circuit relaxation period of 60 min to allow the cell potential to approach quasi-equilibrium.

The lithium-ion diffusion coefficient (D_{Li^+}) was calculated using the classical short-time slab-diffusion model proposed by Weppner and Huggins[7,8], expressed as:

$$D = \frac{4}{\pi\tau}\left(\frac{m_{AM}V_M}{M_{AM}S}\right)^2\left(\frac{\Delta E_s}{\Delta E_t}\right)^2$$

Where, D: Diffusion coefficient of Li ion ($cm^2\ s^{-1}$), τ: pulse time (s), m_{AM}: mass of the active material (g), V_M: molar volume of active material ($cm^3\ mol^{-1}$), M_{AM}: molar mass (g), **S:** geometrical surface area (cm^2), ΔE_s: Voltage change in relaxation time (V), ΔE_t: Voltage change in time pulse (V), L: Diffusion length (cm).

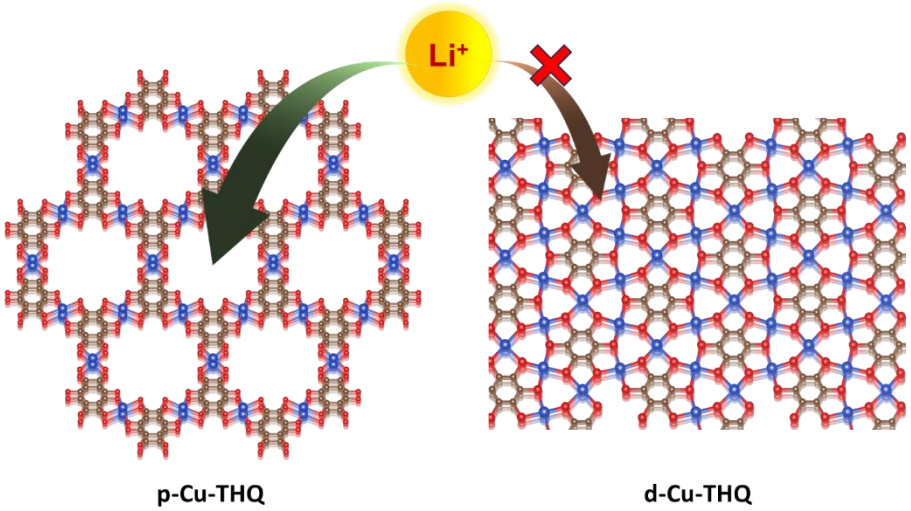

Figure S13. Schematic illustration of diffusion-dominated lithium-ion transport in porous p-Cu-THQ and surface-controlled (capacitive) charge storage in dense d-Cu-THQ.

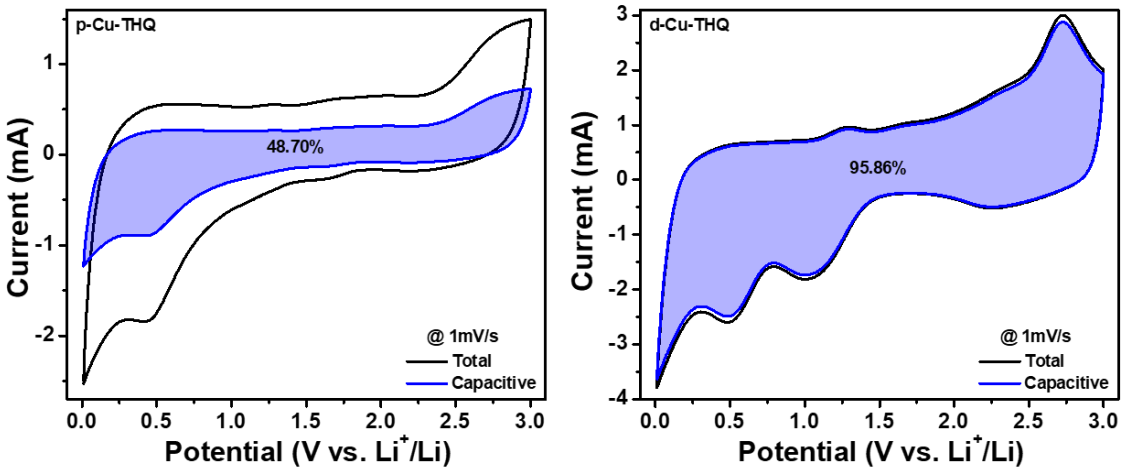

Figure S14. Separating the capacitive current and diffusive current at a scan rate of 1 mV s^{-1}.

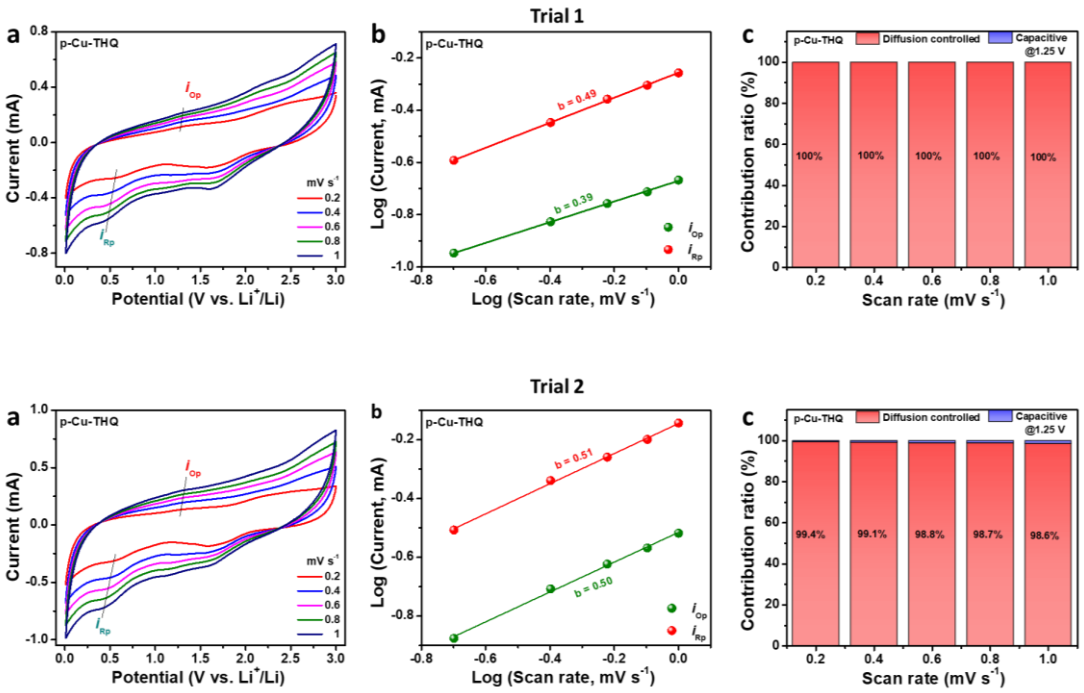

Figure S15. (a) Cyclic voltammetry at 0.2, 0.4, 0.6, 0.8 and 1 mV s^{-1}**, (b)** b-values of different peaks and **(c)** Capacitive-contribution ratios at different scan rates for p-Cu-THQ.

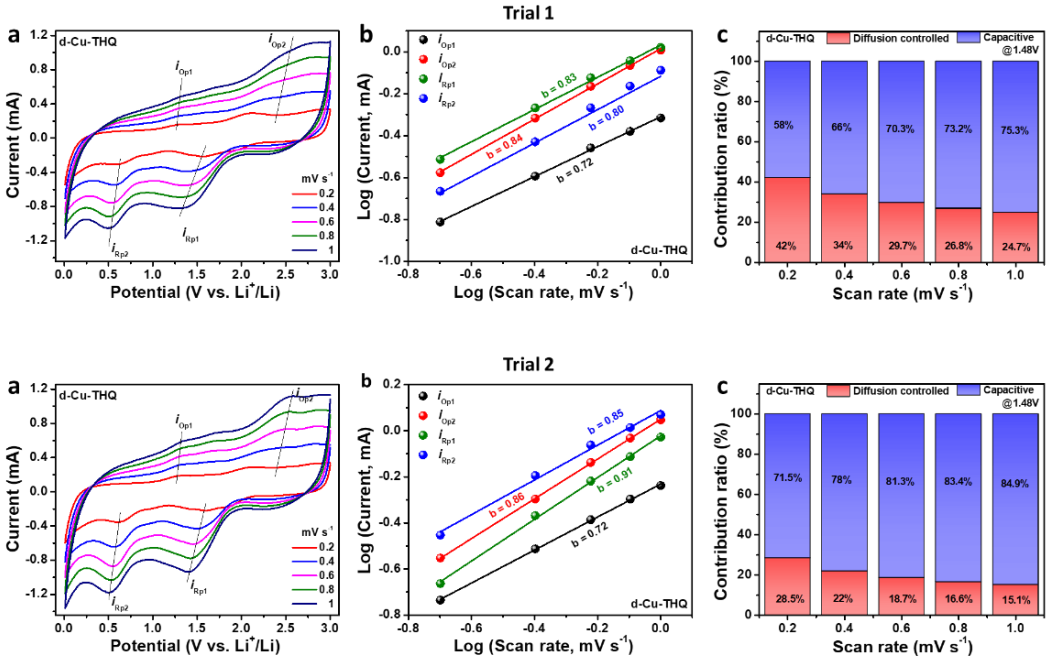

Figure S16. (a) Cyclic voltammetry at 0.2, 0.4, 0.6, 0.8 and 1 mV s^{-1}**, (b)** b-values of different peaks and **(c)** Capacitive-contribution ratios at different scan rates for d-Cu-THQ.

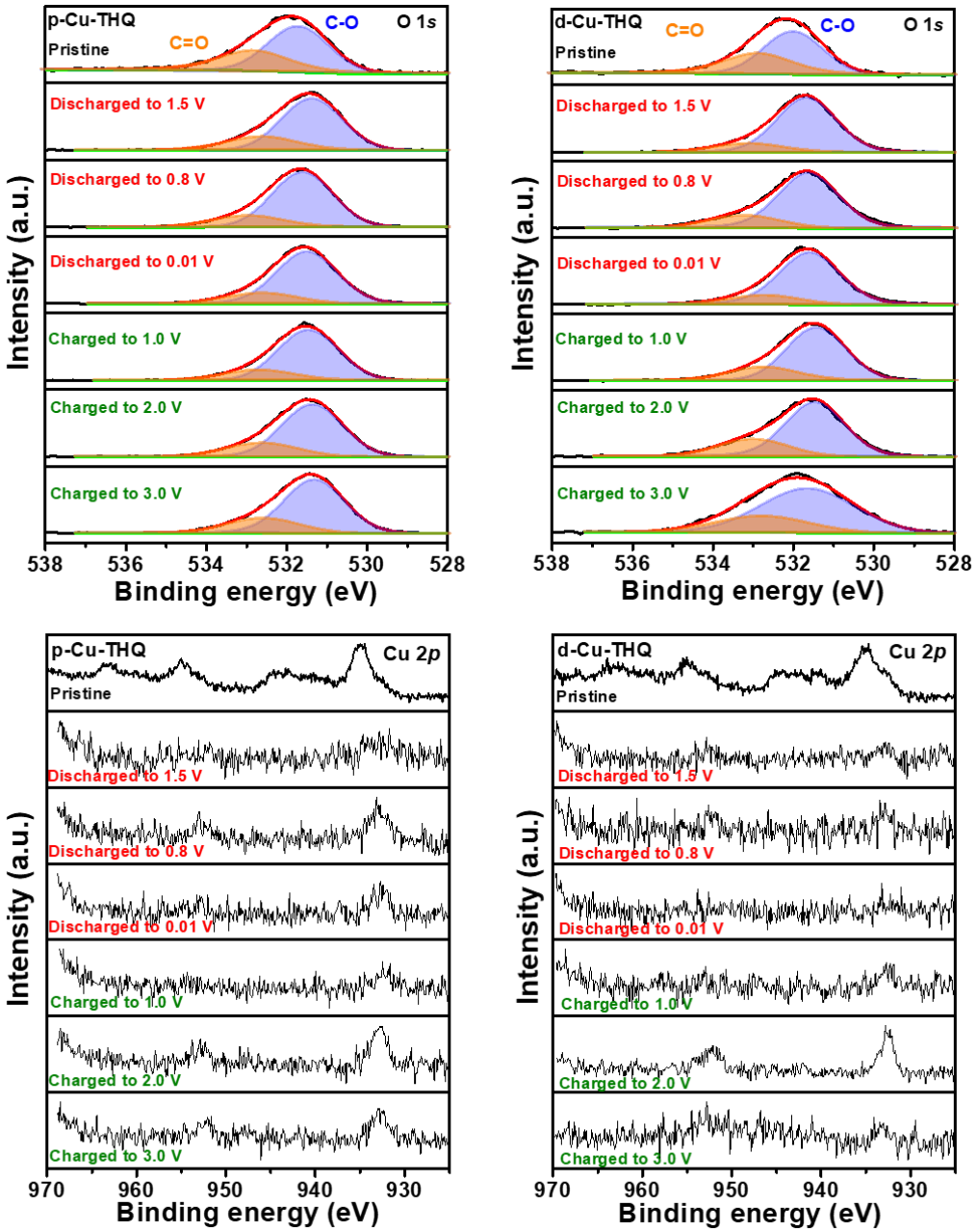

Figure S17. X-ray photoelectron spectroscopy (XPS) analysis of Cu 2*p* and O 1*s* for p-Cu-THQ (left panel) and d-Cu-THQ (right panel) electrodes recorded at different discharge/charge states.

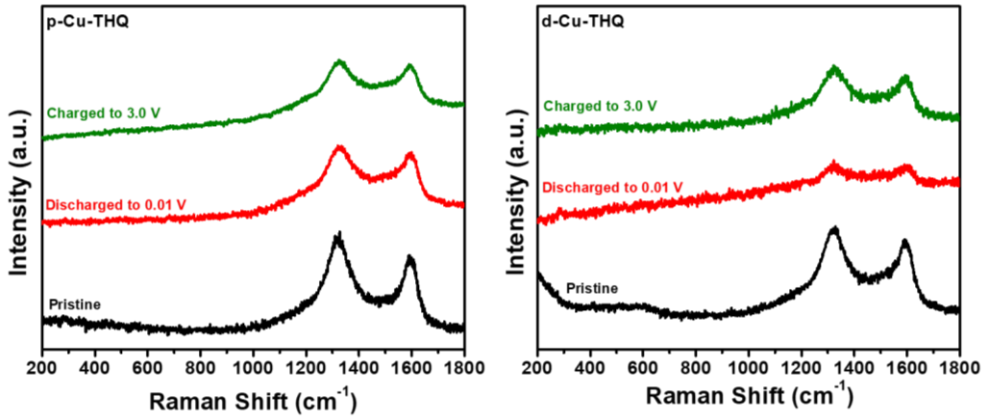

Figure S18. Raman spectroscopy for p-Cu-THQ (left panel) and d-Cu-THQ (right panel) electrodes recorded at pristine, charged (3.0 V) and discharged (0.01 V vs. Li^+/Li) states. Raman signatures from the electrodes were predominantly exhibiting strong D and G bands originating from the conducting additive, largely diminishing the active material's Raman features.

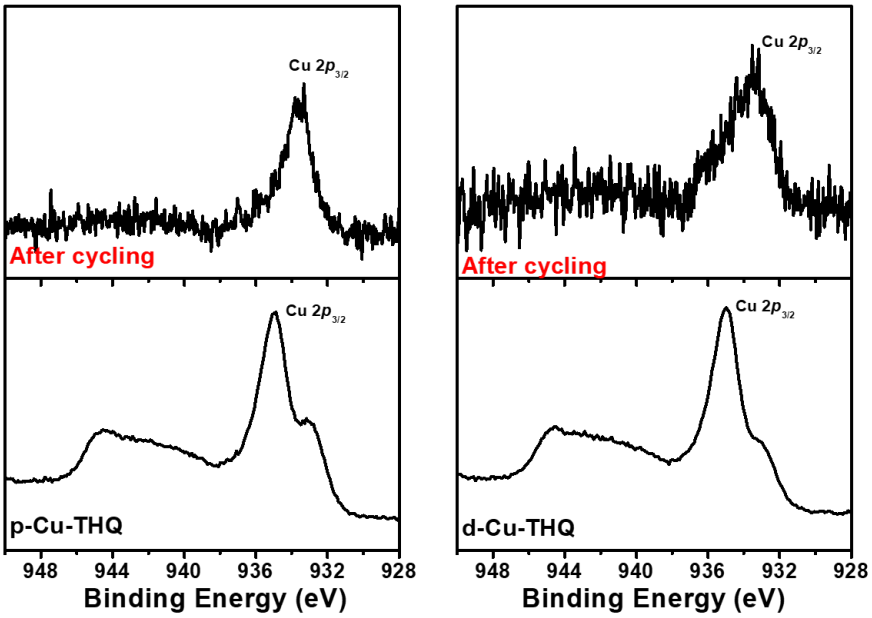

Figure S19. Post-cycling Cu 2*p* XPS spectra of p-Cu-THQ and d-Cu-THQ electrodes.

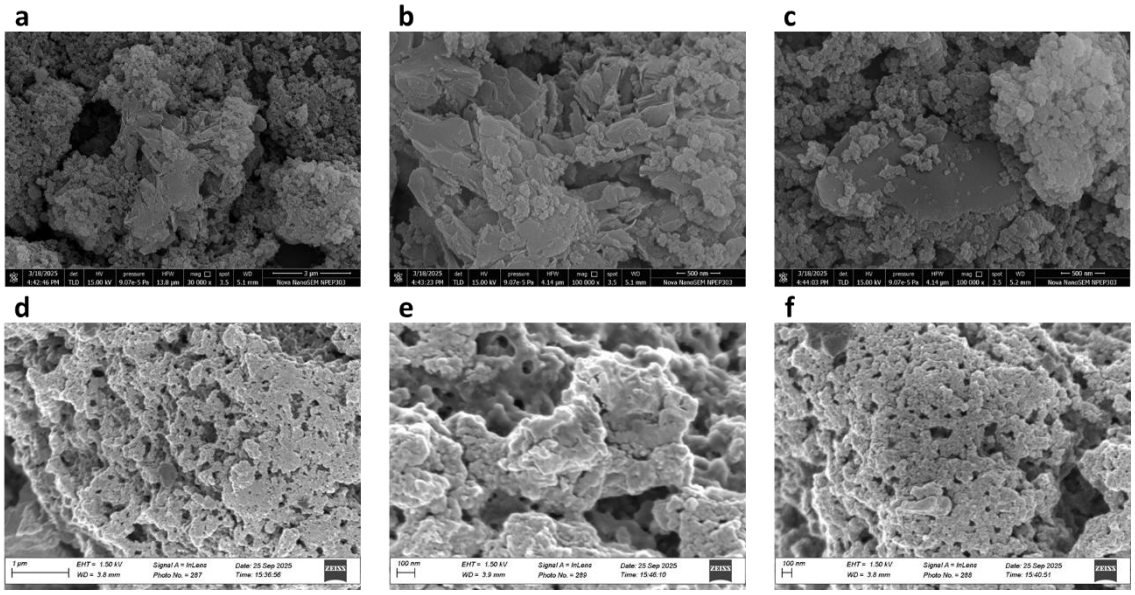

Figure S20. SEM images of **(a,b,c)** p-Cu-THQ powder samples and **(d,e,f)** after cycling.

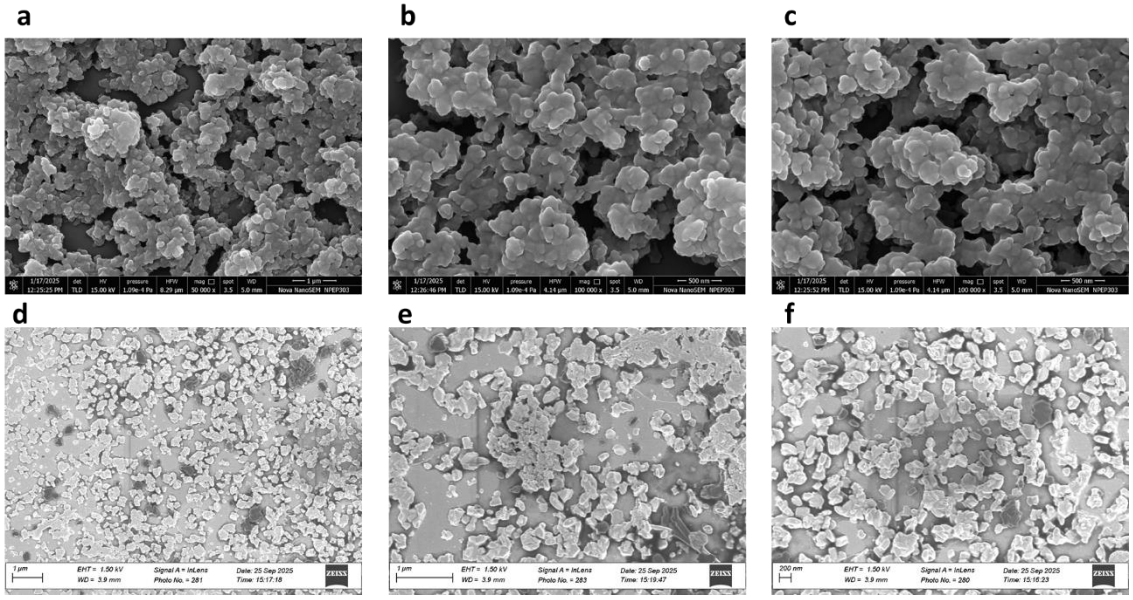

Figure S21. SEM images of **(a,b,c)** d-Cu-THQ powder samples and **(d,e,f)** after cycling.

Table S1: Comparison of Cu-THQ LIB anodes with other 2D MOF LIB anodes.

Sample	Loading (mg cm^{-2})	Electrolyte	Operating voltage	Initial Capacity (CC/DC/R)	Cycling Stability (RC/R/CN)	Reference
p-Cu-THQ	**~0.8-0.9**	**1M $LiPF_6$ in EC/DMC/EMC (1:1:1)**	**0.01-3.0 V**	**(740/1379/100)**	**(~785/100/300)**	**This work**
d-Cu-THQ	**~0.8-0.9**	**1M $LiPF_6$ in EC/DMC/EMC (1:1:1)**	**0.01-3.0 V**	**(739/1537/100)**	**(~321/100/300)**	**This work**
Cu-HATN	~0.7-1	1 M $LiPF_6$ in EC/DMC/DEC (1:1:1)	0.01-3.0 V	(621/1177/50)	(687/300/600)	3
Cu-TAC	~0.8-1	1 M $LiPF_6$ in EC/DEC/DMC (1:1:1)	0.01-3.0 V	(910/1373/50)	(641/300/600)	4
Cu_3(HHTP)(THQ)	1-1.2	1 M $LiPF_6$ in EC/DEC/DMC (1:1:1)	0.01-3.0 V	(705/1219/50)	(625/300/200)	5
Cu-HHTQ	~1-1.5	1 M $LiPF_6$ in EC/DMC/DEC (1: 1: 1)	0.01-3.0 V	(989/1716/15)	(658/600/200)	6
rGO/Cu–BHT	1.5-2	1 M $LiPF_6$ in EC/DMC/DEC (1: 1: 1)	0.01-3.0 V	(--/1384/500)	(1131/500/400)	7
Co-CAT MOF	--	1 M $LiPF_6$ in EMC/EC/DMC (1:1:1)	0.01-3.0 V	(1213/1672/200)	(800/200/200)	8
Cu-CAT	~1.1	1 M $LiPF_6$ in EC/DEC (1:1)	0.01-3.0 V	(713/1011/200)	(646/200/320)	9
Ni-CAT	~1	--	0.01-3.0 V	(982/1440/200)	(626/200/200)	10
Cu-HHTP/G	1.5	1 M $LiPF_6$ in EC/DEC	0.01-3.0 V	(1141/1699/100)	(1086/100/300)	11
$Ni_3(HITP)_2$	2	1 M $LiPF_6$ in EC/DMC (1:1)	0.005-3.00 V	(662/1080/50)	(700/50/70)	12
$Ni_3(HITP)_2$	0.9-1.2	1 M $LiPF_6$ in EC/DMC (1:1)	0.01-3.0 V	(1078/1555/100)	(501/2000/500)	13
2D Ni-MOF	--	1 M $LiPF_6$ in EC/DEC (1:1)	0.01-3.0 V	(--/1809/100)	(765/100/140)	14
Sn-PMA	2.6	1 M $LiPF_6$ in EC/DEC/DMC (1:1:1)	0.01-3.0 V	(600/1567/100)	(541.3/200/100)	15

CC, charge capacity (mAh g^{-1}); DC, discharge capacity (mAh g^{-1}); R, rate (mA g^{-1}) RC, reversible capacity (mAh g^{-1}); R, rate (mA g^{-1}); CN, cycling number.

References

1. M. Tian, R. Qiao, G. Cen, L. Tian, L. Ben, H. Yu, M. De Volder, C. Zhao, Q. Wang and X. Huang, *Nat. Commun.*, 2025, **16**, 6864.
2. M. Han, J. Liu, C. Deng, J. Guo, Y. Mu, Z. Zou, K. Zheng, F. Yu, Q. Li, L. Wei, L. Zeng and T. Zhao, *Adv. Energy Mater.*, 2024, **14**, 2400246.
3. J. Yin, N. Li, M. Liu, Z. Li, X. Wang, M. Cheng, M. Zhong, W. Li, Y. Xu and X.-H. Bu, *Adv. Funct. Mater.*, 2023, **33**, 2211950.
4. J.-C. Yin, X. Lian, Z.-G. Li, M. Cheng, M. Liu, J. Xu, W. Li, Y. Xu, N. Li and X.-H. Bu, *Adv. Funct. Mater.*, 2024, **34**, 2403656.
5. J.-C. Yin, Y.-Q. Zhang, Z.-G. Li, M. Cheng, M. Liu, W. Li, N. Li and X.-H. Bu, *Sci. China Mater.*, 2023, **66**, 4566-4574.
6. J. Yan, Y. Cui, M. Xie, G.-Z. Yang, D.-S. Bin and D. Li, *Angew. Chem. Int. Ed.*, 2021, **60**, 24467-24472.
7. C. Meng, P. Hu, H. Chen, Y. Cai, H. Zhou, Z. Jiang, X. Zhu, Z. Liu, C. Wang and A. Yuan, *Nanoscale*, 2021, **13**, 7751-7760.
8. P. Mao, H. Fan, C. Liu, G. Lan, W. Huang, Z. Li, H. Mahmoud, R. Zheng, Z. Wang, H. Sun and Y. Liu, *Sustain. Energy Fuels*, 2022, **6**, 4075-4084.
9. L. Guo, J. Sun, W. Zhang, L. Hou, L. Liang, Y. Liu and C. Yuan, *ChemSusChem*, 2019, **12**, 5051-5058.
10. L. Guo, J. Sun, X. Sun, J. Zhang, L. Hou and C. Yuan, *Nanoscale Adv.*, 2019, **1**, 4688-4691.
11. X. Yin, Y. Li, W. Cai, C. Fan, W. Liu, N. Wang, G. Qin, Z. Xie, X. Chen and Y. Han, *Appl. Surf. Sci.*, 2023, **624**, 157124.
12. Y. Zhang, T. Qiu, F. Jiang, S. Amzil, Y. Wang, H. Fu, C. Yang, Z. Fang, J. Huang and G. Dai, *Appl. Surf. Sci.*, 2021, **556**, 149818.
13. A. Nazir, H. T. T. Le, A.-G. Nguyen and C.-J. Park, *Electrochim. Acta*, 2021, **389**, 138750.
14. L. Zhang, X. Zhang, D. Han and S. Wu, *Inorg. Chem. Commun.*, 2023, **158**, 111511.
15. S.-B. Xia, L.-F. Yao, H. Guo, X. Shen, J.-M. Liu, F.-X. Cheng and J.-J. Liu, *J. Power Sources*, 2019, **440**, 227162.